Effect of Depth Implantation of Lanthanum on The Oxidation of $Fe_{80}Cr_{20}$ based Alloys

Darwin Sebayang, Hendi Saryanto, Pudji Untoro, Deni Shidqi Khaerudini

Abstract*—The aim of this study is to investigate the effect of depth implantation of lanthanum on the oxidation of $Fe_{80}Cr_{20}$ alloys. Intermetallic FeCr was developed by mechanical alloying technique with milling time 40 h and 60 h respectively and followed by hot compaction process at a temperature of 1273 K and pressure of 25 MPa. The specimens were implanted with Lanthanum dopant with doses of 10^{17} ions/cm^2 with different depth due to different density. Isothermal oxidizing behaviors of $Fe_{80}Cr_{20}$ alloys was carried out in a resistance heated furnace in 1 atm of laboratory air at constant at temperatures of 1173 K and 1273 K. X-ray diffraction (XRD) and Scanning Electron Microscopy (SEM) followed by Energy Dispersive X-ray spectroscopy (EDX) analysis were used to examine the microstructure, morphology characterization and the influence of lanthanum dopant and its influence on the formation of oxides layer of specimens after oxidation process. The oxide scales formed on both specimens at 1173 K in which consisted of thin chromia (Cr_2O_3) dan FeO with a composition similar percentage. Lanthanum mainly existed in the outer surface of Cr_2O_3 oxide film in the form of La_2O_3 and La_2CrO_6. Meanwhile, the oxide scale formed at 1273 K mainly consisted of α-$(FeCr)_2O_3$, α-La_2CrO_6, and γ-Fe_2O_3. With different dopant concentration in the surface depth of specimens, it will cause the formation of different oxidation layer on the surface of the specimens after oxidation.

***Keywords*—Fe-Cr, Oxide Layer, Lanthanum, X-ray Diffraction.**

I. Introduction

Iron-based alloys have received much attention for potential application as SOFC interconnects. Traditionally, Fe-based steels with additions of chromium have been used as high (up to 1273 K) temperature applications [1], where oxidation or corrosion resistance is required. Therefore, their stabilization and oxidation behavior at high temperature are vital to actual applications. The addition of chromium to the alloy is made primarily to promote the formation of a dense, adherent layer of Cr_2O_3 on the surface of the alloy [2].

Chromium is by far the most important alloying element in stainless steel production. A minimum of 10.5% chromium is required for the formation of a protective layer of chromium oxide on the steel surface [3]. However, Chromium dioxide that forms on chromium containing alloys becomes non-protective upon exposure to oxidizing atmospheres for extended periods at high temperatures. This is due mainly to crack formation in the oxide caused by growth, thermal stresses and due to formation of volatile Cr_2O_3 [4].

The iron-chromium system has long been used as the basis of many engineering alloys for high-strength, corrosion-resistant applications. To enable practical applications of mechanical alloying, it is necessary to predict how the milling progress is affected by such parameters as the amount of material being processed or type of the ball mill used [5]. The end product depends on many parameters such as the milling conditions. By mechanical alloying process we succeeded to develop a smaller crystallite size on nano scale [6].

The protection of high temperature alloys and coating against oxidation is provided by the formation of slow growing oxide films, which often consist of Cr_2O_3. One major limiting factor in the protection is extensive oxide loss from the surface, or oxide spalling under thermal cycling condition. It has been known for many years that the minor addition of oxygen active element, such as Hf, La, Y, and Ce, could significantly improve the spallation resistance of these oxide scales [7], [8].

Several protection methods have been proposed to minimize evaporation of volatile Cr-species, such as coating of the interconnect materials. Ion Implantation offers the possibility to introduce a controlled concentration of an element to a thin surface layer rapidly. It is first shown, as in [9], that chromium implantation improved the corrosion resistance of iron. Reference [10] shows that the La-implantation also has succeeded the implantation of La with various depths on the $Fe_{80}Cr_{20}$ substrate. The La was implanted on one of the coupons faces with doses of 10^{17} ions/cm^2 on the area of 8.03 cm^2 and ion beam energy of 100 keV.

Refer to [11] analyzed the effect of lanthanum implantation on the surface of $Co_{60}Cr_{40}$. However, it focused only on measuring the binding energy changes of element Cr caused by La-implantation and did not investigate the influence of depth profile to oxidation behavior. Therefore, in this study, the effect of depth lanthanum implantation on oxidation behavior on $Fe_{80}Cr_{20}$ will be examined.

II. Experimental Methods

The received specimens of $Fe_{80}Cr_{20}$ were manufactured with different milling time alloys followed by hot compaction process at 1173 K and pressure of 25 MPa. The density of each sample was measured using Archimedes method. The lanthanum was then implanted on one of the coupons faces specimens with doses of 10^{17} ions/cm^2 on the area of 8.03 cm^2 and ion beam energy of 100 keV. The

This work was supported in part by the Advanced Manufacturing and Materials Center (AMMC) - Universiti Tun Hussein Onn Malaysia (UTHM) through the Fundamental Research Grant Scheme (FRGS) project of the Ministry of Higher Education - Malaysia under grant vot no. 0361.

Darwin Sebayang is with the Advanced Manufacturing and Materials Center (AMMC), Faculty of Mechanical and Manufacturing Engineering, Universiti Tun Hussein Onn Malaysia, 86400, Parit Raja, Batu Pahat, Johor Bahru, Malaysia (darwin@uthm.edu.my).

Pudji Untoro is with Center for Technology of Nuclear Industry Material, National Nuclear Energy Agency (BATAN), Kawasan Puspiptek Serpong Gd.43 Tangerang 15314, Banten, Indonesia (untoro@batan.go.id)

density value and the depth profile of dopant ions on the surface of each specimen are showed in Table 1.

Table.1. Density value and depth profile of as received materials $Fe_{80}Cr_{20}$ [10].

Sample	Density value (g/cm^3)	Depth profile (Å)
$Fe_{80}Cr_{20}$ with milling time 40 h (Called FeCr 40 h)	7.0619	276
$Fe_{80}Cr_{20}$ with milling time 60 h (Called FeCr 60 h)	6.5496	297

The microstructure and percentage of element obtained by EDX on the specified point of the implanted specimens is shown in Fig 1 and Fig 2. The EDX results for the percentage of elements of implanted samples are listed in Table 2.

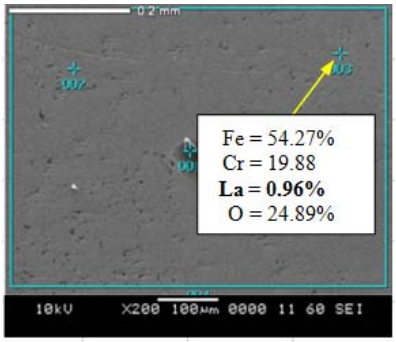

Fig.1. Surface morphology of FeCr 40 h after Implantation process

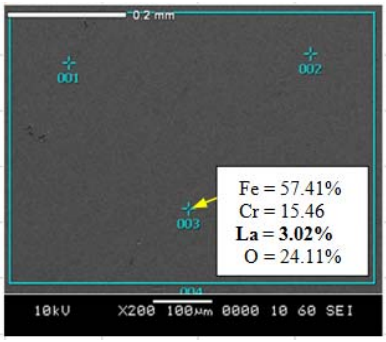

Fig.2. Surface morphology of FeCr 60 h after Implantation process

Table 2 summarizes the percentage of elements for both types of specimens. It shows that the percentage of Lanthanum dopant on the substrate of FeCr 60 h was greater than the FeCr 40 h. It concludes that the percentages as well as the depth profile are greater.

Table.2. Percentage of an element for both types of specimens

Elements	Percentage Of Elements	
	FeCr 40 h	FeCr 60 h
O	24.89%	24.11%
Fe	54.27%	57.41%
Cr	19.88%	15.46%
La	0.96%	3.02%

The specimens were then oxidized in pressure of 1 atm of laboratory air at constant temperature of 1173 K and 1273 K for 100 hours. The samples were weighted at each 20 hours by an electronic microbalance with a weighting accuracy of 0.01 mg. The samples weight change was recorded after each cycle to plot the weight change vs. oxidation time graph to observe the oxidation kinetics. X-ray Diffraction (XRD) and scanning electronic microscopy (SEM) coupled to an Energy dispersive spectrometer (EDX) were used to examine the surface morphology and phase composition of oxide films.

III. RESULTS AND DISCUSSION

A. Oxidation Kinetic

The oxidation kinetic of FeCr 40 h and FeCr 60 h are plotted in Fig.3 and Fig.4, respectively, at the oxidation temperature of 1173 K and 1273 K.

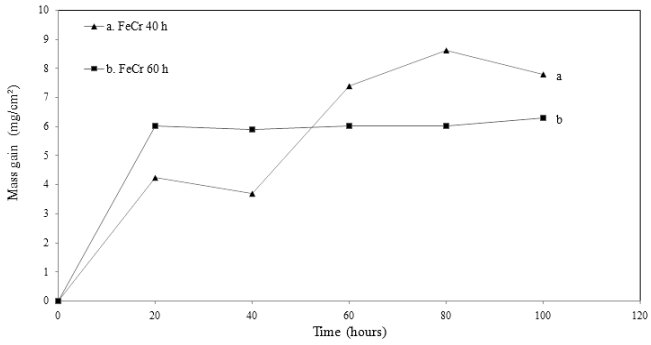

Fig.3. Mass gain vs. time for isothermal oxidation of FeCr 40 h and FeCr 60 h at 1173 K.

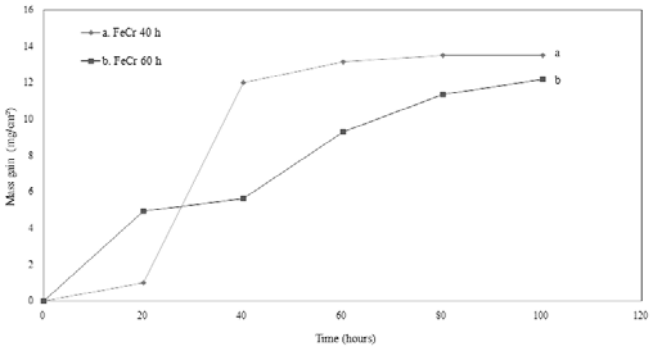

Fig.4. Mass gain vs. time for isothermal oxidation of FeCr 40 h and FeCr 60 h at 1273 K.

The oxidation kinetic at temperature 1173 K and 1273 K showed that the FeCr 60 h exhibited the lowest oxidation rate.

B. Parabolic Rate

The parabolic rate constant (k_p) is determined by the mass gain per unit surface area of a specimen and exposure time (t) [12].

$$(\Delta W/A)^2 = k_p t \qquad (1)$$

where k_p is the parabolic rate constant. The k_p was obtained from the slope of a linear regression fitted line of $(\Delta W/A)^2$

ISBN: 978-988-18210-7-2
ISSN: 2078-0958 (Print); ISSN: 2078-0966 (Online)

vs. t plot. Fig.5 and Fig.6 shows the fit of the parabolic rate law for the isothermal oxidation of FeCr alloys at 1173 K and 1273 K.

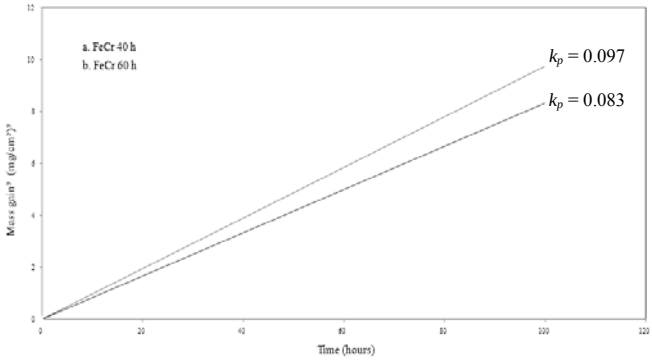

Fig.5. Parabolic rate of FeCr 40 h and FeCr60 h at 1173 K.

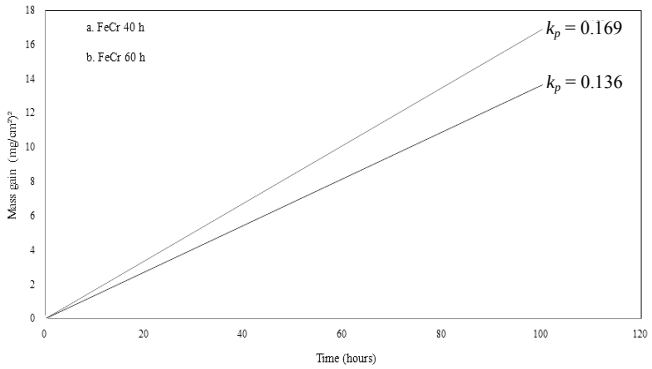

Fig.6. Parabolic rate of FeCr 40 h and FeCr60 h at 1273 K.

The parabolic rate constants (k_p) at oxidation temperature 1173 K and 1273 K showed that the FeCr 60 h exhibited the lowest k_p of 0.083 $mg^2cm^{-4}s^{-1}$ and 0.136 $mg^2cm^{-4}s^{-1}$ respectively. It seems that deeper lanthanum dopant influences to the substrate reducing the oxide scale and it will be further analyzed in C.

C. Identification of Oxide Phases

Fig. 7 and Fig. 8 as well as Table 3 show the phases of oxide layers from XRD analysis.

The Ellingham diagram and phase diagram of FeCr [13] were used to identify the oxides phase formed during oxidation at different temperatures and to explain the oxidation phase for a qualitative interpretation of the oxidation mechanism accurately. The partial pressure at 1173 K and 1273 K are approximately 10^{-8} - 10^{-25} atm and 10^{-6} - 10^{-22} atm, respectively. It was obtained using the equilibrium oxygen partial pressure (pO_2). Detail explanations of identification of oxide phase can be seen at [13].

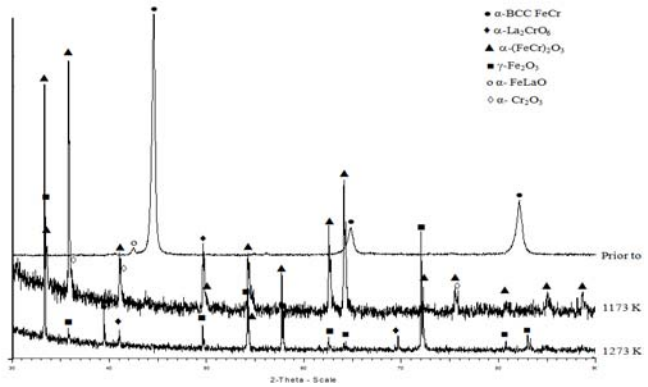

Fig.7. Diffraction patterns of FeCr 40 h prior to and after oxidation at temperatures 1173 K and 1273 K.

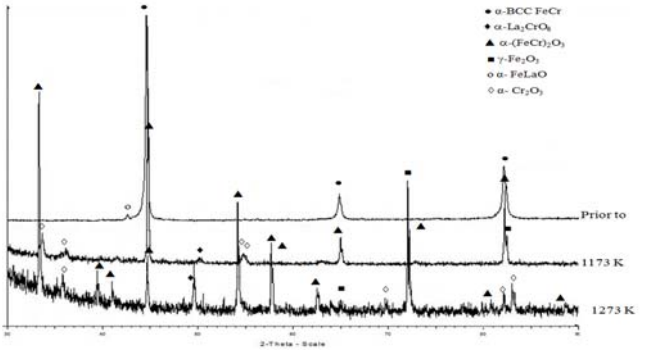

Fig.8. Diffraction pattern of FeCr 60 h prior to and after oxidation at temperatures at 1173 K and 1273 K.

Table 3. Identification of oxide phase after oxidation.

Alloys Type	1173 K	1273 K
FeCr 40 h	α-$(FeCr)_2O_3$ α-Cr_2O_3 α-La_2CrO_6	α-$(FeCr)_2O_3$ γ-Fe_2O_3 α-La_2CrO_6
FeCr 60 h	α-$(FeCr)_2O_3$ α-Cr_2O_3 α-La_2CrO_6	α-$(FeCr)_2O_3$ α-Cr_2O_3 γ-Fe_2O_3 α-La_2CrO_6

The implanted phase prior to oxidation of FeCr alloys were mainly α-BCC-FeCr and small amount of α-FeLaO, as shown in Fig.7 and Fig.8.

After oxidation at 1173 K, α-$(FeCr)_2O_3$ and α-Cr_2O_3 with rhombohedral structure were the main oxidation scale for both specimens, but α-La_2CrO_6 with orthorhombic structure showed as minor oxidation scale. For both specimens after oxidation at 1273 K, α-$(FeCr)_2O_3$, α-La_2CrO_6, and γ-Fe_2O_3 were identified as main oxidation scale, but α-Cr_2O_3 showed only at FeCr 60 h as the deeper implanted specimen. This implies that the depth implantation influences in the protection of Cr_2O_3 scale. It was proven by the formation of α-La_2CrO_6 peaks for both specimen type that formed at 1173 K and 1273 K of two peaks, respectively.

D. Morphology and microcomposition of oxide scale

The microstructure and EDX pattern of the oxide scale phases on the oxidized alloy surface are shown in Fig 9, Fig 10, Fig 11, and Fig 12. It also lists the EDX of the oxide scale phases on the oxidized alloy surface, as shown in Table 4.

ISBN: 978-988-18210-7-2
ISSN: 2078-0958 (Print); ISSN: 2078-0966 (Online)

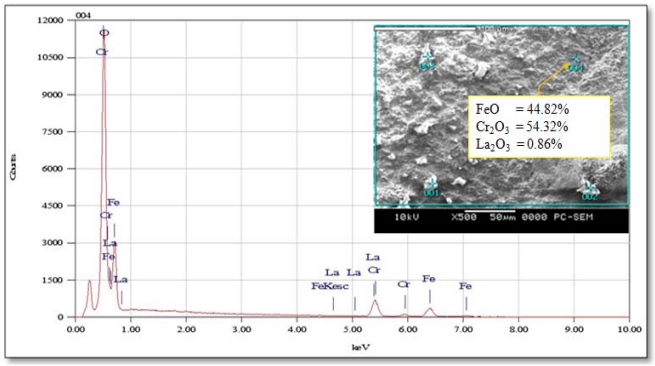

Fig.9. Oxide morphology of FeCr 40 h after oxidation at 1173 K for 100 h.

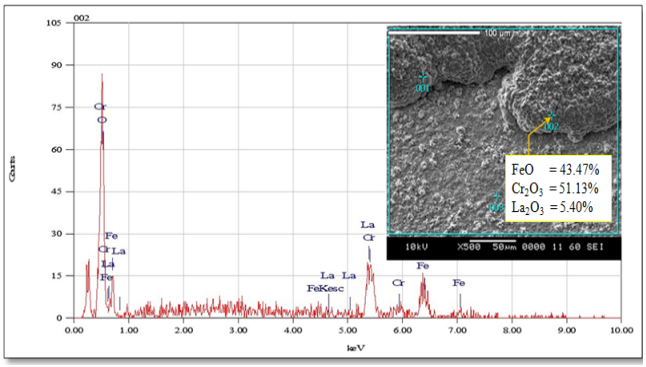

Fig.12. Oxide morphology of FeCr 60 h after oxidation at 1273 K for 100 h.

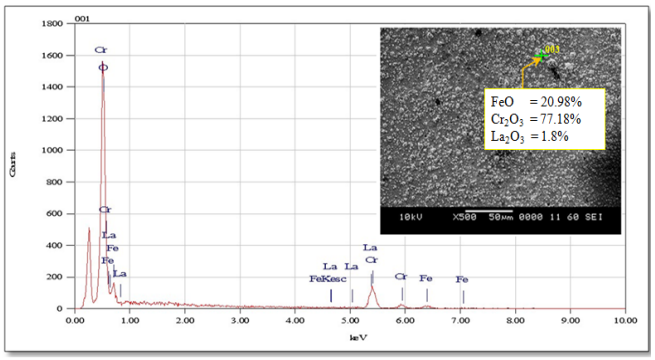

Fig.10. Oxide morphology of FeCr 60 h after oxidation at 1173 K for 100 h.

After oxidation at 1173 K, the oxide formed on the surface of alloys type specimen, as shown in Fig.7 and Fig.8, looked grain finer. This phenomenon was explained due to chromia growth mechanism, where chromium preference diffused outward to react with oxygen. The thin oxide scales showed that they mainly consisted of chromium oxide (Cr_2O_3) and iron oxide (FeO) with a small amount of lanthanum oxide (La_2O_3) of the oxide scale.

The oxide formed on the surface of all alloys type at 1273 K is shown in Fig.9 and Fig.10. It showed the relatively large concentration of iron oxide for FeCr 40 h, but the EDX did not identify the presence of La_2O_3 at this substrate. This indicates that the formation of iron rich oxides beneath a dense chromia scale may occur if the chromia scale becomes unstable in equilibrium with the alloy chromia. Meanwhile, the instability of chromia has led to the increasing growth of iron oxide, thus causing the crack in the oxide layer as shown in Fig.9.

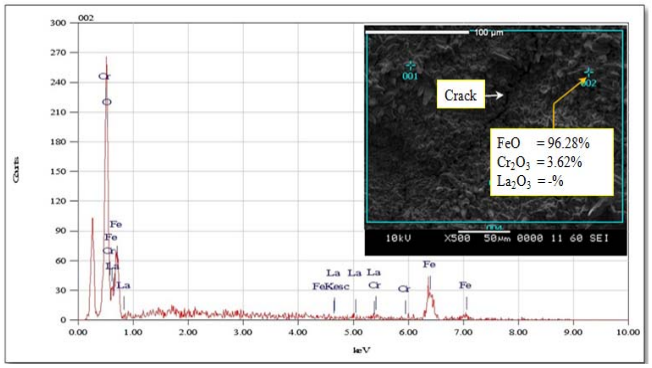

Fig.11. Oxide morphology of FeCr 40 h after oxidation at 1273 K for 100 h.

Tabel 4. Percentage of oxide phase, identified by EDX

Oxide Layer	1173 K		1273 K	
	FeCr 40 h	FeCr 60 h	FeCr 40 h	FeCr 60 h
FeO	44.82%	20.98%	96.28%	43.47%
Cr_2O_3	54.32%	77.18%	3.62%	51.13%
La_2O_3	0.82%	1.8%	-	5.4%

Table 4 summarizes the percentage of oxide phase for both types of specimens. It showed that the differences of the depth lanthanum implantation influenced the oxide scale formed. On the oxide scale of the FeCr 40 h after oxidation at 1173 K showed that with the differences of the depth of lanthanum implantation, the presence of La_2O_3 of 1.8% exhibited the lowest compared with specimen FeCr 60 h. Similarly, for oxidation at 1273 K the presence of La_2O_3 on the oxide scales of FeCr 60 h at 5.40% has the biggest percentage composition of La_2O_3 compared to FeCr 40 h at 0%. This effect means that the deepest lanthanum implantation is able to increase Cr_2O_3 crystal formation rate, particularly on the FeCr 60 h and promote the formation of Cr_2O_3 oxide phase. Lanthanum also inhibited [Cr^{3+}] ion diffusion within Cr_2O_3 oxide film, which can be partially confirmed by the increase of the Cr binding energy after a long time of oxidation, and change the oxidizing rate-controlling step from predominant [Cr^{3+}] cation outwards diffusion to predominant [O^{2-}] anion inward diffusion.

IV. Conclusions

1. Surface depth implantation of specimens does not seem to have much difference in the oxide layer formation, but the difference is in the percentage of oxide phase formation.
2. Lanthanum dopant implanted more deeply better affects the protection of the Cr_2O_3 scale on the oxide surface layer. The presence of lanthanum has influenced the formation stable layer of Cr_2O_3 and plasticity as well as protects it from evaporation and cracks on high temperature oxidation.

References

[1] R.N. Basu, *Recent Trend in Fuel Cell Science and Technology*. New Delhi, India: Jointly published Springer and Anamaya Publishers, 2007, pp. 260.

[2] S.C. Singhal and K. Kendall, *High-temperature solid oxide fuel cells: Fundamentals, Design and Applications*. Oxford, UK: Elsevier Ltd., 2003.

ISBN: 978-988-18210-7-2
ISSN: 2078-0958 (Print); ISSN: 2078-0966 (Online)

[3] G.W. Meetham and M.H. Van de Voorde, *Materials for High Temperature Engineering Applications.* Berlin: Springer-Verlag, 2000, ch.5.
[4] M.F. Pillis, O.V. Correa, E.G. de Araújo, and L.V. Ramanathan, "Oxidation behavior of FeCr and FeCrY alloys coated with an aluminium based paint," *Journal of Materials Research*, vol. 11, no. 3, 2008, pp. 251-256.
[5] C. Suryanarayana, "Mechanical alloying and milling," *Journal of Progress in Materials Science*, Elsevier Science Ltd., vol. 46, 2001, pp.1-184.
[6] P. Untoro, D. Sebayang, and H. Saryanto "Development of $Fe_{80}Cr_{20}$ based alloy by mechanical alloying process and combined with ultrasonic technique," *Proceedings of 7th Asean Microscope Conference 2009*, BATAN, 3 – 5 Dec. 2009.
[7] K. Hilpert, W. J. Quadakkers, and L. Singheiser,"Interconnector," in *Handbook of Fuel Cells – Fundamentals, Technology and Application*, Chichester: John Wiley & Sons, Ltd., vol. 4, Part 8, 2003, pp. 1037–1054.
[8] F.Y. Hou, and J. Stringer, "Effect of surface applied reactive elements on the early stage," *Journal de Physique IV*, vol. 3, Dec. 1993, pp. 231-239.
[9] G. Marest, "Surface treatment by ion implantation," *Journal of Hyperfine Interactions*, vol. 111, no.1-4, Dec. 1998, pp. 121-127.
[10] H. Saryanto, D. Sebayang, and P. Untoro, "Ion implantation process of lanthanum and titanium dopants into a substrate of $Fe_{80}Cr_{20}$," *Proceedings of the Malaysian Metallurgical Conference '09 (MMC'09)*, Universiti Malaysia Perlis (UMP), 1-2 Dec. 2009.
[11] H. Jin, X. Zhou, and L. Zhang, "Effects of lanthanum ion-implantation on microstructure of oxide film formed on Co-Cr alloy," *Journal of Rare Earths*, Elsevier Ltd., vol. 26, no. 3, Jun. 2008, pp. 406 – 409.
[12] C.H. Xu, W. Gao, and H. Gong, "Oxidation behaviour of FeAl intermetallics: The effects of Y and/or Zr on isothermal oxidation kinetics," *Journal of Intermetallics*, Elsevier Ltd. vol. 8, 2000, pp. 769 – 779.
[13] L. Mikkelsen and S. Linderoth, "High temperature oxidation of iron-chromium alloy," *Journal of Materials Science and Engineering*, Elsevier Ltd., vol. A361, 2003, pp. 198–212.

ISBN: 978-988-18210-7-2
ISSN: 2078-0958 (Print); ISSN: 2078-0966 (Online)